

High Field Imaging – An Overview of Technical Challenges.

Paul R. Harvey Ph.D.

Philips Medical Systems, The Netherlands.

Email: paul.harvey@philips.com

Educational Objective.

To describe physical phenomena and specific innovations that are important for clinical imaging at high field strengths ($\geq 3T$), including those related to MRI safety at high field, optimized pulse sequences, and other technical challenges.

Introduction.

The development of clinical MRI has been an ongoing process since the early 1980's. Initial clinical systems utilized resistive magnet technology and operated at field strengths on the order of 0.15T. Within a few years, the availability of superconductive magnet technology enabled the development of magnets operating around the 0.5T field strength. In 1984, the first 1.5T clinical systems appeared. At about the same time, a number of manufacturers were also experimenting with 2.0T and 4.0T, whole-body size, systems. These early high field systems, while used mostly for head imaging, provided much of the insight into the physical problems of performing MRI, on human subjects, at magnetic field strengths significantly higher than 1.5T (1).

Three physical limitations were identified almost immediately:

- The issue of RF penetration and its associated impact on the specific absorption rate (SAR).
- The issue of increased magnetic susceptibility and its impact on image quality.
- The issue of the changing NMR relaxation behavior and its impact on image contrast and imaging efficiency.

In addition to these physical differences, some technology limitations prevented the further wide-spread adoption of high field systems at that point in time. These included:

- The size and cost of the superconducting magnet technology (not only to buy, but also to operate and maintain).
- The lack of availability of suitably high performance, and physically robust, gradient system hardware.
- The lack of availability of suitably high performance data acquisition hardware.

- The immaturity in the design of RF coils with respect to operation at high frequencies without negative influence from the patient load.
- The relative immaturity of available imaging methods and correction schemes.
- Multi-channel RF reception capability was not available until the early 1990s (2).
- Parallel imaging was not available until the late 1990s (3,4).
- The regulatory conditions to operate such systems on a patient population were either not in place or too restrictive.

By 2005, more than 20 years later, most of the required innovations have been made to enable clinical whole-body imaging at a field strength of 3.0T.

This segment of the study course will explore the critical boundary conditions and physical requirements on various aspects of the design of a high field MRI system. It will be shown that all of the insight, and many of the innovations, that have accumulated in the past 20 years are a basic requirement to achieve acceptable clinical performance at an operating field strength of 3.0T. Based on the current experience at 3.0T an optimum path to realize improved image quality and performance at higher field strengths will become apparent.

The Physical Limitations of Different Field Strengths.

Signal To Noise Ratio (SNR).

If we explore the physical limitations of operating at different field strengths, it becomes apparent that they are different in each case. Consider, for example, a system operating at 0.15T.

The system signal to noise (SNR) can be represented by the following relation:

$$SNR \propto \frac{S_{NMR}}{\sigma_n} \quad [1]$$

Where S_{NMR} , the NMR signal, is given by

$$S_{NMR} = \omega_0^2 \cdot N \cdot \chi \cdot \frac{V_h}{\gamma} \quad [2]$$

This expression, derived in reference (5), includes the signal dependencies on resonant frequency, ω_0 , voxel volume, $V_h = dx \times dy \times dz$ and number of turns on the receiver coil. The standard deviation of the noise can be represented by the following expression:

$$\sigma_n = \sqrt{\frac{2 \cdot K \cdot \Gamma \cdot R}{T}} \quad [3]$$

This expression includes the noise dependencies on the effective resistance properties, R , of sample and RF coil and sample temperature, Γ . K is the Boltzman constant and the parameter T is the acquisition sampling time which relates the noise dependency to image bandwidth.

It is worthwhile looking further into the effective resistance R . The value R contains both sample (patient) resistance R_p and coil resistance R_c properties (6).

$$R = R_p + R_c \quad [4]$$

R_c describes the electrical resistance of the conductors used for the receiving coil. It can be shown that R_c is related to the physical dimensions of the receiving coil, the properties of the conductor (usually copper) and the NMR frequency of operation (field strength). This relationship is described using the 'skin effect'. As the frequency increases, the current in the RF coil flows more on the surface of the conductors and less in the center. The effective available cross-section of the conductor is reduced and the resistance increases accordingly.

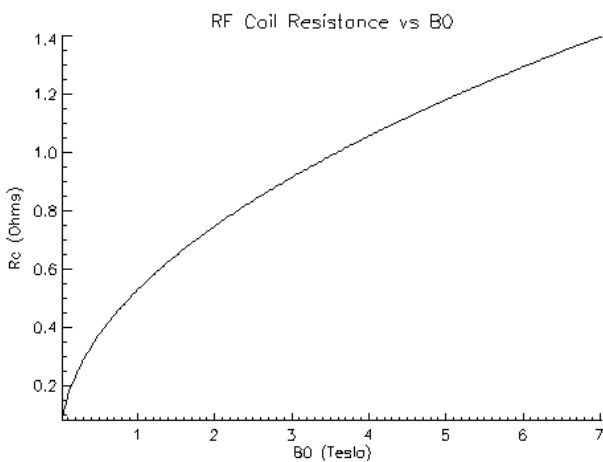


Figure 1 – Coil resistance (R_c) vs field strength.

Figure 1 shows the relationship for a 5 turn solenoid coil of radius 10 cm, length 20 cm. The conductor width is assumed to be 1 cm. The thickness is allowed to match the optimum skin depth at each frequency.

The effective resistance due to the patient load, R_p , is derived with the help of reciprocity (5). R_p is related to the average power dissipated in the sample:

$$W_{av} = \frac{I_p^2 \cdot R_p}{2} \quad [5]$$

Where, for a simple solenoid,

$$W_{av} = \omega_0^2 \cdot \mu_0^2 \cdot N^2 \cdot I_p^2 \cdot \left(\frac{\pi \cdot l \cdot r_0^4 \cdot \sigma}{16} \right) \quad [6]$$

represents the average power dissipated in a conducting sample due to a sinusoidal voltage applied to a coil surrounding it. l and r_0 describe the coil length and radius. σ is the conductivity of the sample (human tissue). I_p is the peak current flowing in the coil. For unity current:

$$R_p = \omega_0^2 \cdot \mu_0^2 \cdot N^2 \cdot \left(\frac{\pi \cdot l \cdot r_0^4 \cdot \sigma}{8} \right) \quad [7]$$

By making reasonable assumptions about sample conductivity it is possible to estimate the value of R_p for the same coil dimensions used to estimate R_c above. It is now instructive to compare the ratio of R_p/R_c as a function of field strength.

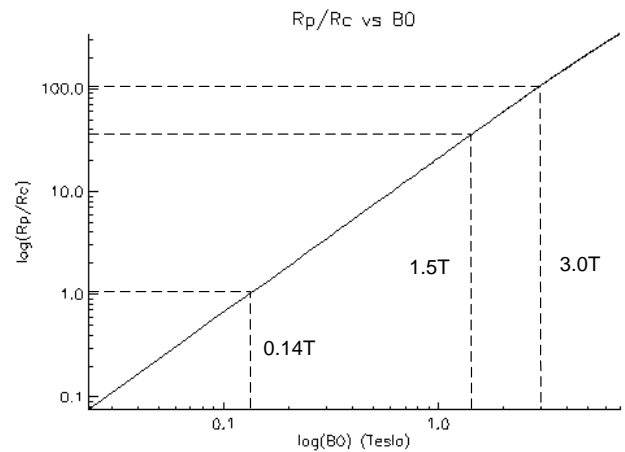


Figure 2 – R_p/R_c versus field strength.

Figure 2 shows that, above about 0.15T, the patient (sample) induced contributions to the noise dominate over the thermal noise introduced by the conductor forming the receiving coil.

Ignoring, for the time being, the differences in NMR relaxation properties that occur with changing field strength, and assuming scalability of the RF hardware with respect to noise performance, it is possible to estimate the relative change in SNR as a function of field strength. For fixed scan parameters, the expected SNR relationship, as a function of field strength, is shown in figure 3.

SNR is essentially linearly proportional to field strength.

For the same scan parameters, the SNR at 0.15T is at least a factor 20 times lower than at 3.0T. Since the noise is inversely proportional to the square root of scan time, the factor in scan time required to increase SNR by a factor 20 is 400. Thus, a scan which takes 3 minutes on a 3.0T system would need to run for 20 hours on a 0.15T system in order to achieve the same SNR!

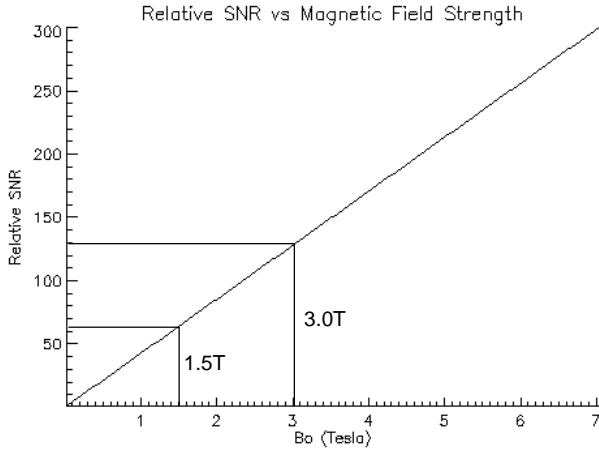


Figure 3 – Relative SNR versus field strength.

So, a clear physical limitation of operating at a field strength of 0.15T is the achievable signal to noise ratio (SNR).

As field strength is increased, other limiting factors come into play. Primarily, the specific absorption rate (SAR).

From SNR to SAR (Specific Absorption Rate).

The Specific Absorption Rate (SAR), in the MRI context, is a measure of the power absorbed by the human body when exposed to a time varying magnetic field (B_1) in the radio frequency band. SAR is broadly defined by the relationship:

$$SAR_{body} = \frac{Power_{body}}{Mass_{body}} \quad [8]$$

and is expressed in the unit of W/kg.

The oscillating B_1 field created by a sinusoidally varying current in an RF coil can be represented as:

$$B_1(t) = \mu_0 \cdot N \cdot I_p \cdot \cos(\omega_0 \cdot t) \quad [9]$$

Expressed slightly differently

$$B_1(t) = B_{1pk} \cdot \cos(\omega_0 \cdot t) \quad [10]$$

Where

$$B_{1pk} = \mu_0 \cdot N \cdot I_p \quad [11]$$

Combining this insight with equation [6] above yields

$$W_{av} = \omega_0^2 \cdot B_{1pk}^2 \cdot \left(\frac{\pi \cdot l \cdot r_0^4 \cdot \sigma}{16} \right) \quad [12]$$

From equation [8] it is possible to write

$$SAR_{whole-body} = \frac{W_{av}}{M_{patient}} \quad [13]$$

which can be used to show that

$$SAR \propto \omega_0^2 \cdot B_{1pk}^2 \quad [14]$$

For a constant RF coil volume, it was shown in the previous section that

$$SNR \propto \omega_0 \quad [15]$$

The physical mechanisms that are fundamentally involved in the definition of SNR, and its dependency with increasing field strength, are the very same mechanisms that result in patient heating from SAR related power deposition! Notably, given the same fixed scan parameters, the rate at which SAR related power deposition increases with field strength quickly outpaces the rate of SNR gain.

All things being equal, it should be clear that, in order to realize the time saving benefits that the increased SNR of high field promises, it is essential to find ways of circumventing the faster increasing SAR related power deposition before it exceeds the limit that a human patient can withstand.

B_1 Amplitude and The Practical Control of SAR.

It is instructive to investigate what real B_{1pk} requirements might be in practice. A starting point may be a demanding sequences, like a flow compensated spectral-spatial binomial water only excitation (7) as illustrated in figure 4.

Under such constraints, to achieve a 6 mm slice thickness at a field strength of 3.0T requires a B_{1pk} of 21 μ T, a gradient amplitude of 29 mT/m and a gradient slew rate in the region of 200 T/m/s.

Assuming a human head of mass 4.2 kg, from equations [12] and [13] it is possible to estimate the SAR for the head (for continuous exposure at a peak B_1 field of 21 μ T). The SAR at 3.0T would be about 136 W/kg. At 1.5T the same conditions would yield a continuous SAR of 35 W/kg.

Regulatory requirements (8) require that, in case of head imaging, the average SAR over 6 minutes does not exceed 3.2 W/kg. The basis of this requirement (and all SAR limits) comes from the need to limit temperature rise during scanning to less than 1 degree.

A scan operating at a peak B₁ field of 21 μT and a duty cycle of 2.3% is a perfectly reasonable situation to find in practice. Most RF amplifiers are not specified to operate beyond 10% duty cycle at maximum power. With the aid of modern imaging techniques, including variable flip angle and parallel imaging methods, most clinical scans can be made to operate efficiently within these requirements.

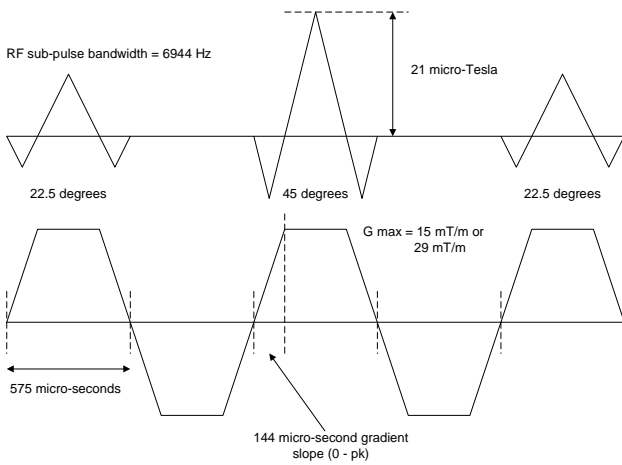
SAR and the Patient.

There are a number of ways to estimate the SAR on a per patient basis:

- One approach is to measure the change in forward and reflected power to the transmitting RF coil, with and without the patient in place. This gives an estimate of the power absorbed by the patient for a fixed RF flip angle. If the RF duty cycle and mass of the patient is known, the SAR can be calculated. Some vendors use a power meter to track the average power delivered to the RF coil. Based on calibrating the proportion absorbed by the patient, and estimating the mass of the patient, it is possible to limit SAR exposure.
- An alternative method calibrates the system power to deliver a known B₁ amplitude. For a given transmit coil geometry it is possible to show that the absorbed power is essentially linear with patient mass (the load). The slope of this graph is a constant which can be used to directly relate the SAR, for a patient of any size, to the B₁ and duty cycle used in the imaging sequence. The advantage of this approach is that nothing is assumed about the mass of the patient and all estimation of SAR can be performed without requiring calibration data.

At low field strength, where head SAR and whole-body SAR have been of primary interest, either of the approaches to SAR control can suffice. At higher operating field strengths, numerical simulations, using Finite Difference Time Domain (FDTD), have shown that the local SAR limits are reached sooner than the whole-body limits (9). When this is the case, the empirical methods described above fail to provide enough insight into the appropriate limits at which to operate the MRI system.

The author has found a combination of the second approach, together with knowledge derived from FDTD simulations (of a variety of possible patient orientations inside the MRI system) to be advantageous with respect to SAR control on a clinical 3.0T system. In addition, the use of FDTD simulations during the hardware design stage can enable much more SAR efficient designs of the system body coil. This topic will be expanded further during the presentation.



Gradient spec. T/m / s	Max. gradient ampl. in 144 μs mT/m	Minimum slice thickness Mm	Max. B ₁ for 90 degree. μT
21.3/0.2	15	11	21
40.0/0.2	29	6	21

Figure 4 – RF and gradient requirements at 3.0T.

It is fairly straightforward to show that a change in temperature

$$\Delta T = \frac{SAR \cdot \tau}{C_{head}} \quad [16]$$

of 1 degree can occur for a SAR of 3.2 W/kg, τ = 360 seconds and where an approximate specific heat capacity for the head is C_{head} ~ 1152 J/kg.C.

An MRI system rarely needs to deliver the peak B₁ amplitude with 100% duty cycle. It would be dangerous to do so. Clearly, a SAR of 136 W/kg (as calculated above) is far too high. The calculation of SAR therefore needs to include the duty cycle. The steady-state SAR is thus

$$\overline{SAR} = SAR_{100\%} \cdot \eta \quad [17]$$

Where SAR_{100%} represents the continuous SAR, given a fixed B₁ amplitude and η is the RF duty cycle. So, in the example above, for the scan operating at a peak B₁ of 21 μT, the RF duty cycle required to meet the head SAR limits of 3.2 W/kg is

$$\eta = \frac{3.2}{136} = 0.023 = 2.3\% \quad [18]$$

Modern Methods for Calculating SAR.

As mentioned above, at high field, simply determining bulk SAR (head or whole-body) from absorbed power measurements on a per patient basis almost guarantees that the local SAR limits will be exceeded. Thus, at 3.0T, the situation can arise where the whole-body SAR is at or below the required 4 W/kg and the local SAR is considerably beyond the limit. Volunteer studies have shown that, when the local SAR limits are exceeded, the subject very rapidly becomes very uncomfortable (10).

There are different meanings to the term “local SAR”. It can mean:

1. The SAR as a result of the electric field resulting from capacitive coupling of the patient’s skin to a component of the transmitting coil. This can be avoided in a well designed coil.
2. The local SAR within the body as a result of the internal electric field distribution generated by the exposure to uniform RF transmission from a volume RF coil. This is less easy to avoid because, at high fields, the electrical properties of the human body determine, almost completely, the RF distribution within.

For the latter definition, numerical methods such as the FDTD (11, 12) can be used to determine an accurate SAR distribution according to the relationship

$$SAR = \frac{\sigma |E|^2}{\rho} \quad [19]$$

Where σ represents the tissue conductivity and ρ the tissue density (both spatially varying). E is the electric field induced in the tissue by the changing B_1 field. By reference to Maxwell’s equations and Faraday’s law of induction, it can be shown that eq. [19] is essentially equivalent to the application of Ohms law to determine the induced power per unit mass resulting from the application of the oscillating B_1 field.

The validity of such FDTD simulations has been illustrated through a comparison of temperature measurements made on a saline sphere with a simulation of the same arrangement (13).

Concentrating on the latter definition of “local SAR”, figure 5 shows the simulated difference in B_1 field distribution, at 3.0T, for two body transmit coils of different lengths.

What is immediately apparent is that the longer body coil doesn’t realize any better RF uniformity than the shorter body coil! This phenomenon was also observed in practice by D. Alsop et al (14).

Another observation, derived from simulations, is that the use of a longer body coil results in a significantly higher whole-body and local SAR deposition (up to 50% higher). This is coupled with a higher power requirement and a lower SNR! (15).

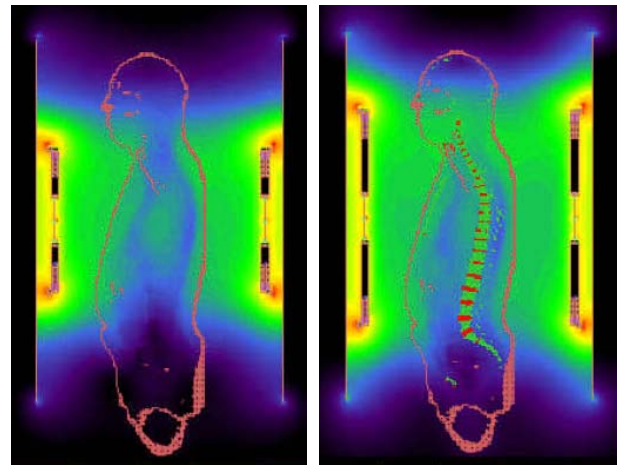


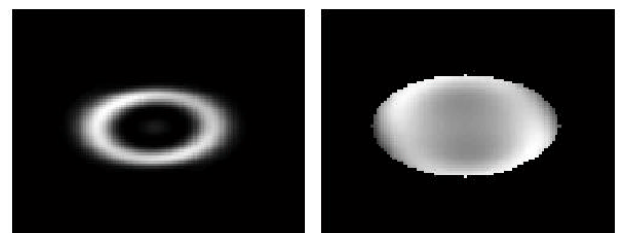
Figure 5 – B_1 uniformity vs Coil length.

Thus, another important caveat of high field system design is that bigger is not always better.

The approach to obtaining the best possible performance from a transmitting RF coil at 3.0T goes beyond ensuring its ideal operation in free space. It requires careful attention to the design and its impact within the human subject. To date, the timely use of FDTD simulations have proven essential for this task.

Dielectric Effects and RF Uniformity.

Utilizing FDTD simulation methods it becomes possible to isolate and compare the different effects due to the dielectric properties of the object being imaged. Figure 6 illustrates the effects on uniformity in case of a medium in which permittivity dominates over conductivity and vice versa.



a) $\sigma = 0.03$ S/m, $\epsilon_r = 78$ **b)** $\sigma = 0.5$ S/m, $\epsilon_r = 2.2$

Figure 6 – The competing dielectric effects.

In the case where permittivity dominates, at 128 MHz, the RF wavelength inside the object becomes complex with a length of about 20 cm. For the purely conductive case, the wavelength approaches 27 cm. The primary effect of conductivity results in a shielding effect which reduces

the B_1 amplitude in the center of the object. The permittivity causes a partial focusing effect. In a realistic object (patient), the differing dielectric properties of various tissue compartments leads to a varying combination of both effects.

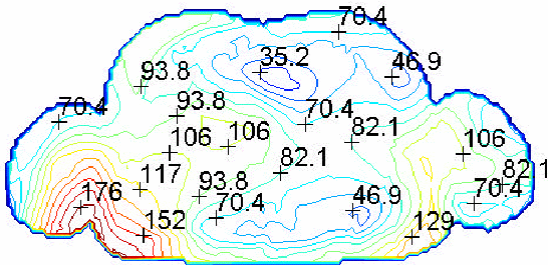


Figure 7 – Flip angle variation in the human body at 128 MHz.

Figure 7 shows the simulated expected flip angle distribution, in a realistic human body model, for a nominal 90 degree excitation at 128 MHz. It is apparent that RF uniformity is mostly determined by the electrical properties of the body. The flip angle range covers 44% – 200% of the desired flip angle. The impact of this extreme lack of uniformity results in image uniformity problems and also failure of spectral fat suppression techniques. Despite this, methods have been developed by which both uniformity and spectral fat suppression can be significantly improved in clinical practice.

Magnet Homogeneity, Bulk Susceptibility, Local Susceptibility and Line-width.

The topic of magnet homogeneity requirements for different field strengths has the potential to lead to confusion.

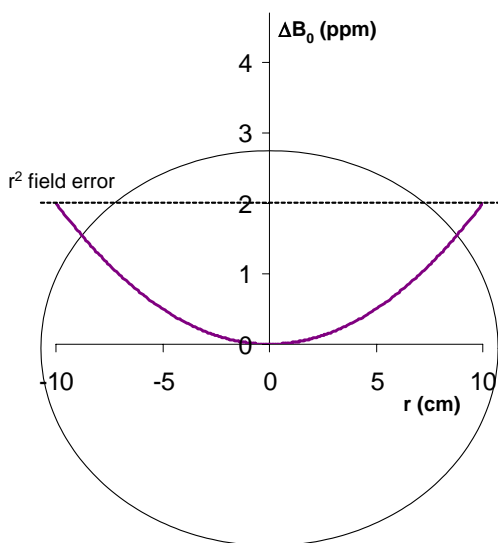


Figure 8 – Homogeneity expressed in ppm.

One of the first points to remember is that the presence of a human body, inside the magnet bore, spoils the homogeneity! This is true irrespective of how good the manufactured bare homogeneity of the magnet is claimed to be.

As the main field strength increases, the potential of the human body to spoil the homogeneity also increases. This is due to the fact that the magnetic susceptibility difference between air and tissue has a fixed ratio. The change of homogeneity this difference induces, in terms of parts per million (ppm), is constant. In terms of absolute magnetic field, however, the inhomogeneity becomes larger with increasing field strength.

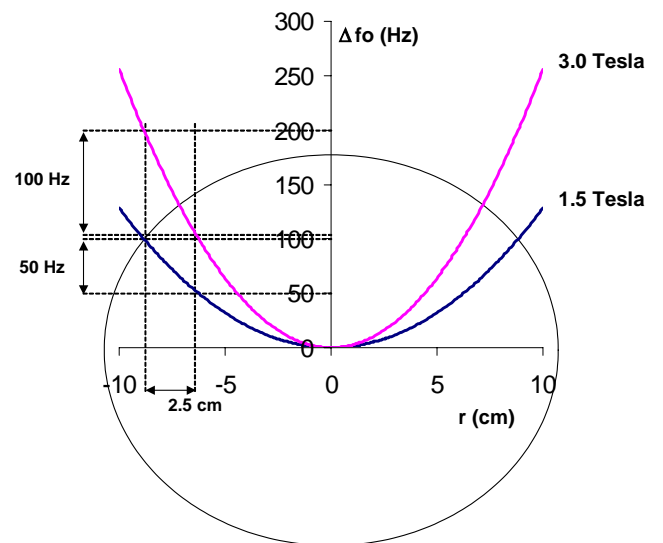


Figure 9 – Homogeneity expressed in Hz.

Figure 8 illustrates a 1D example of the spatially varying (second order) inhomogeneity that might be introduced due to the bulk susceptibility of a human head (the oval shape). Expressed in ppm, it is independent of field strength. Figure 9 shows that, when expressed relative to field strength, the corresponding line-width of a 2.5 cm volume is expected to be twice as broad at 3.0T compared to 1.5T. In this example, the 100 Hz line-width at 3.0T, compared to 50 Hz at 1.5T, effectively negates the improved spectral resolution advantage that is expected from operating at the higher field strength.

It is possible that this situation could be improved by the application of high order shimming, thereby reducing the overall effect of the bulk susceptibility. When contemplating the need for high order shims, it is worth remembering that there are a few “types” of susceptibility!

- “Bulk susceptibility” refers to the effect on homogeneity that the volume of the object has. This results in low order homogeneity variations that can often be corrected by in-vivo shimming.
- The other, more often encountered susceptibility effect is referred to as “local susceptibility”. Problems

attributable to this mechanism are typically found at the inner ear or mouth/air cavities.

A detailed description is beyond the scope of this overview, but it should be realized that the possibility to correct susceptibility effects in-vivo is fundamentally limited by the physical need to place shim coils, or iron shim plates, as close as possible to the interface at which the change of susceptibility occurs. Improving homogeneity over the volume of the whole head represents a different set of boundary conditions compared to improving homogeneity specifically within, for example, the nasal sinuses. The air tissue interface of the nasal sinuses behaves as an additional homogeneity perturbing closed surface within the surface of the head. The possibility to influence the homogeneity at the sinus region, by placing shim coils on the outer surface of the head is fundamentally limited by the fact that the source of inhomogeneity is the air/tissue interface at the sinus itself. This has been recognized in that some researchers have achieved improvements by placing diamagnetic plates inside the mouth of the patient/volunteer (16).

Another way to reduce the effects of susceptibility at higher field strengths is to acquire smaller voxels. This is illustrated in figure 10 in which a voxel width of 1.25 cm is chosen compared to 2.5 cm. In this example, the line-width resulting from the smaller voxel at 3.0T is now 50 Hz. Thus the spectral resolution advantage can be exploited again.

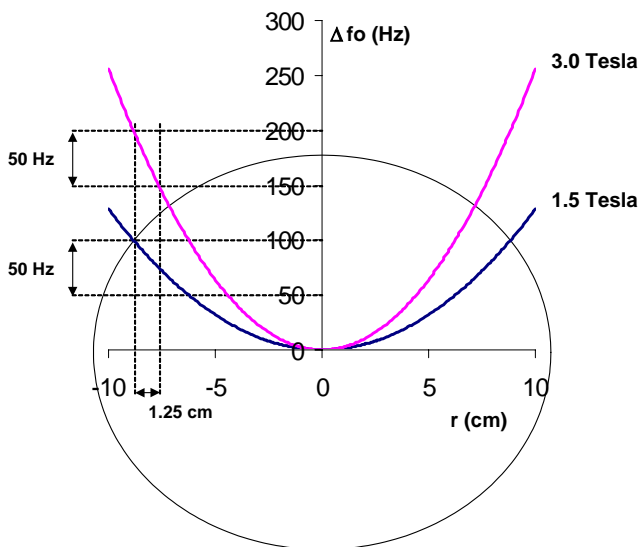


Figure 10 – The effect of reducing voxel size.

On first inspection, it might seem counterproductive to reduce voxel size because this will also reduce the SNR. However, it has been demonstrated that due to the improved T2* resulting from the smaller differential inhomogeneity over the smaller voxel, the SNR reduction turns out not to be as dramatic as a simple linear extrapolation would suggest (17).

So, the broad implication to realize the full advantages for imaging and spectroscopy at higher field strengths, is to acquire smaller voxels – which, fortunately, is exactly the direction in which we wish to go.

The Effect of Line-width Broadening and Geometric Distortion on Image quality.

A study by Thulborn et al (18), compared sensitivity of fMRI at 3.0 Tesla over 1.5 Tesla using two systems with identical gradient performance. The same sequence was used at both field strengths, despite the fact that the absolute magnetic field homogeneity was worse at 3.0T than at 1.5T. They measured bulk T2* values of 50 ms at 1.5T and 25 ms at 3.0T. As expected, the SNR was higher. However, the 3.0T images showed a greater level of geometric distortion. The observed distortion is a direct result of the absolute difference in homogeneity compared to the bandwidth of the EPI data acquisition. In addition to distortion, an effect referred to as “T2* blurring” also occurs. “T2* blurring” is simply a manifestation of the effect of the increased line-width (described above) on image quality. Using the approach described by Farzaneh et al (19) it is possible to illustrate this effect and determine the conditions under which it can be alleviated.

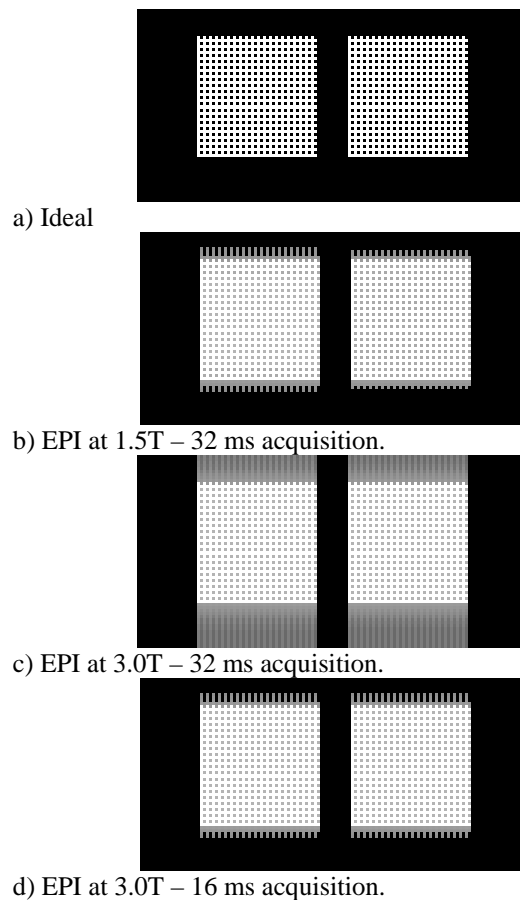


Figure 11 – “T2* Blurring” in EPI versus acquisition time.

Figure 11a is an ideal image and represents two checkerboards. The left checkerboard has a T2 of 90 ms and the right checkerboard has a T2 of 100 ms. It is assumed that EPI is used where the encoding axis is vertical. This simulation calculates the point spread function (PSF) for an EPI acquisition of a given duration and based upon the T2, T2' and hence T2* properties of the objects. It then uses this PSF to simulate the level of T2 broadening, or blurring, that will occur under the particular imaging conditions. Using the values of field homogeneity and T2* quoted by Thulborn et al, figure 11a is the ideal image. Figure 11b represents the level of blurring that would occur for a 32 ms EPI acquisition at 1.5T. Notice that the blurring is only along the encoding axis (as expected for EPI). Figure 11c represents the level of blurring that would occur for the identical 32 ms EPI acquisition at 3.0T. Clearly, the blurring is much worse. This situation can be improved by going to a shorter acquisition time and hence higher gradient performance. Figure 11d illustrates the level of blurring that would occur for a 16 ms EPI acquisition at 3.0T under the same conditions of magnet homogeneity. It is almost identical to the 1.5T example. However, to achieve this in practice, the gradient **amplitude** would have to be **doubled** and the **slew rate quadrupled**. The final SNR would then also take a cut of a factor of $\sqrt{2}$ which can be somewhat improved as a result of the shorter TE that is now possible.

On Gradient Performance Requirements.

Prior to the innovation of parallel imaging (3,4), the usual method of tackling the increasing susceptibility effects at high field was to increase gradient performance. In EPI acquisitions, the improvement is most notable as a result of the reduced time for the echo train readout. This reduction in the duration of the data sampling window translates directly to an increase in image bandwidth (along the encoding axis) which is just equivalent to stating that a higher gradient amplitude was used. Other examples in which the same is true include acquisitions with a short TE in which the fat and water component of the MR signal are in phase. Steady-state imaging sequences require a shorter TR at high fields in order to avoid localized signal loss from inhomogeneity. An added benefit of higher gradient performance, in these kind of scans, is a reduction in scan time and/or an increased slice coverage (provided gradient duty cycle allows).

The negative impact of increased gradient performance is threefold:

- The increased likelihood of Peripheral Nerve Stimulation (PNS).
- The increased acoustic noise and vibration levels.
- The increased cost.

To some extent it is possible to reduce the impact that peripheral nerve stimulation has by using careful choice of gradient waveforms (20) and novel gradient system designs (21). However, these approaches, by now, have

reached their natural limit. All modern MRI systems, irrespective of design, are constrained to operate somewhat below the full capability of the gradient system hardware. For some vendors, the allowed performance is controlled by reference to a PNS model implemented either in hardware (22) or software (23).

Acoustic noise and vibration can be minimized by force balanced design of gradient coils in conjunction with the magnet design. Nevertheless, acoustic noise remains an increasing problem with increasing field strength (24) and both hardware and software methods for mitigation are often required to achieve a practical and safe level of operation.

The added cost required to both increase gradient performance and deal with the side effects now represents a significant portion of the total cost of a MRI system.

While the shortcomings of the some imaging methods cannot be alleviated using parallel imaging alone, as should become apparent, the key to unlocking the full potential of high field imaging is a robust and flexible implementation of a parallel imaging capability. The additional SNR that the higher field provides, when combined with SENSE, can be used to improve image quality beyond anything that is possible using higher gradient performance alone.

Unlocking The Potential of High Field Clinical Imaging.

Having covered a number of the technical challenges facing high field MRI, the next section concentrates on some of the solutions that have been made available to the clinical users of some high field systems.

The Benefits of using Multi-element Receive Coils.

The signal intensity of an MR image is related to the transmit field uniformity and the receive coil sensitivity

$$I(x, y) \propto S_{Tx}(x, y) \cdot S_{Rx}(x, y) \quad [20]$$

Thus, when the same coil is used to transmit as receive, by reciprocity, the “error” in transmit uniformity, due to dielectric effects, is multiplied by the same “error” on the receive sensitivity. This situation can be significantly improved by using separate surface coils to receive. The reason for this improvement is related to the observation that surface coil elements, even at high field, generally exhibit a reduction in sensitivity when moving further from the coil. In contrast, at high fields, a volume birdcage coil, when used to excite the head, will result in a signal peaking in the center of the head due to dielectric focusing effects. Figure 12 illustrates the mechanism for the

improvement in image uniformity when using independent transmit and multi-element receive coils.

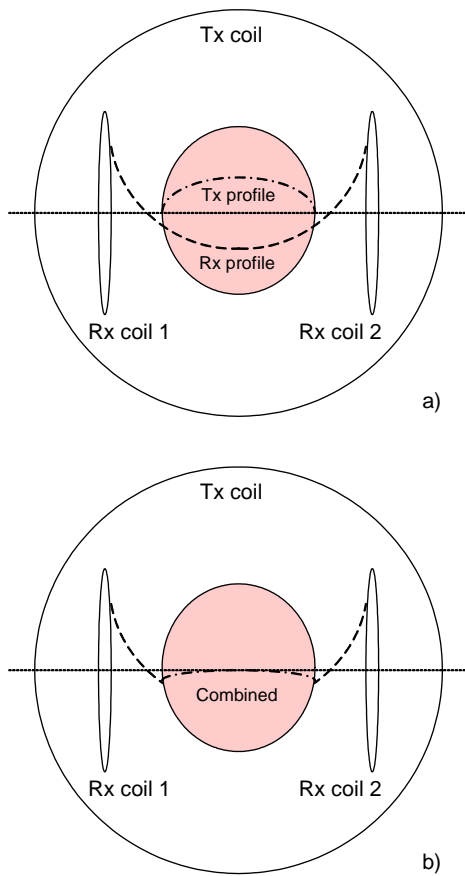


Figure 12 – Separate transmit and receive coils compensate dielectric focusing effects.

The combined sensitivities of the independent transmit and receive coils tend to compensate each other to provide a more uniform image intensity – Figure 12b.

Optimizing Image Contrast in the Presence of Non-uniformity.

RF non-uniformity also has the effect of changing the apparent contrast of an image. Simulations can show that it is often the case that the contrast is not changed significantly, but appears this way because the variation in intensity can become so large. Imaging methods can be made less sensitive to B_1 field uniformity through considered choice of scan parameters such as flip angle. Figure 13 illustrates the improvement on Spin Echo type image uniformity that is possible through careful choice of the excitation flip angle. For this simulation a square “virtual phantom” is used which contains alternating bands of fat, grey, white matter and CSF.

The left most column illustrates the appearance of the virtual phantom under different scanning conditions (Spin Echo) assuming a uniform RF field/sensitivity. The middle column shows the appearance when a non-uniform

transmit field is used (from 40% to 200% of the nominal flip angle). The right most column shows the appearance when a non-uniform transmit and receive sensitivity are used. In Figure 13a a flip angle of 90 degrees is assumed.

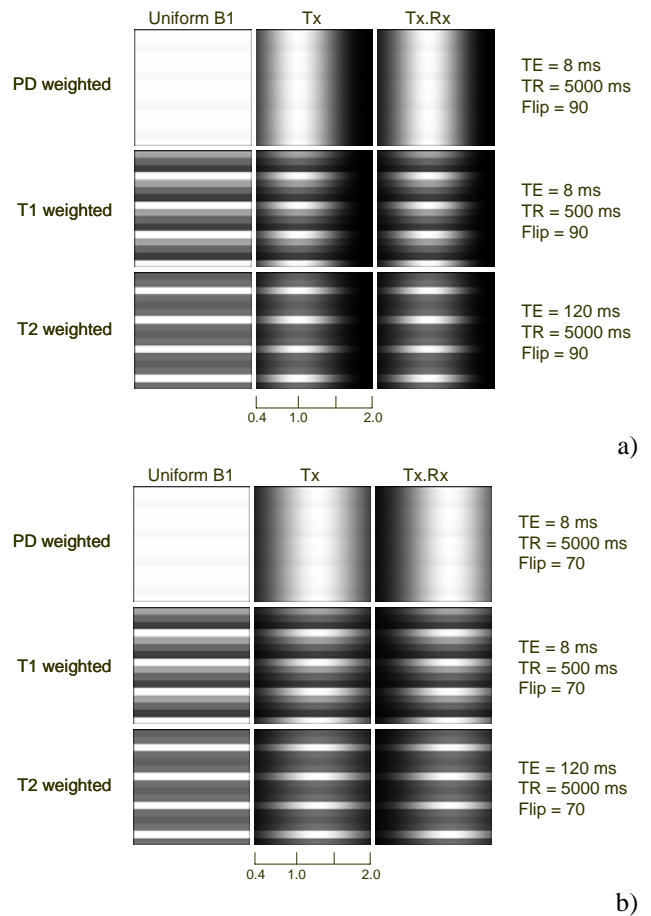


Figure 13 – Uniformity improvement through better flip angle choice.

The contrast between different tissues is not lost, but the intensity is dramatically reduced in some areas. Figure 13b shows that when, for example, a flip angle of 70 degrees is used, the image intensity uniformity can be restored over a larger spread of RF non-uniformity. So, optimization of scan parameters provides yet another route to improved image quality in the presence of both non-uniform excitation and reception.

Flexible RF field Amplitude Control.

It has been noted that, from an MRI protocol perspective, SAR is proportional to both TR (RF duty cycle) and B_1 amplitude. However, the high-level property of an RF pulse, that is most often of interest to the user, is the flip angle. Since the flip angle depends on both the amplitude and duration of an RF pulse, it is possible to realize the same flip angle with different B_1 amplitudes (and RF pulse duration).

Since SAR scales linearly with duty cycle but depends on the square of the B_1 amplitude, lowering the B_1 amplitude

by just a small amount can yield a significant reduction on SAR with little impact on the scan time whilst maintaining a fixed flip angle. Control of the B_1 field, on a per scan basis, turns out to be very advantageous with respect to SAR optimization.

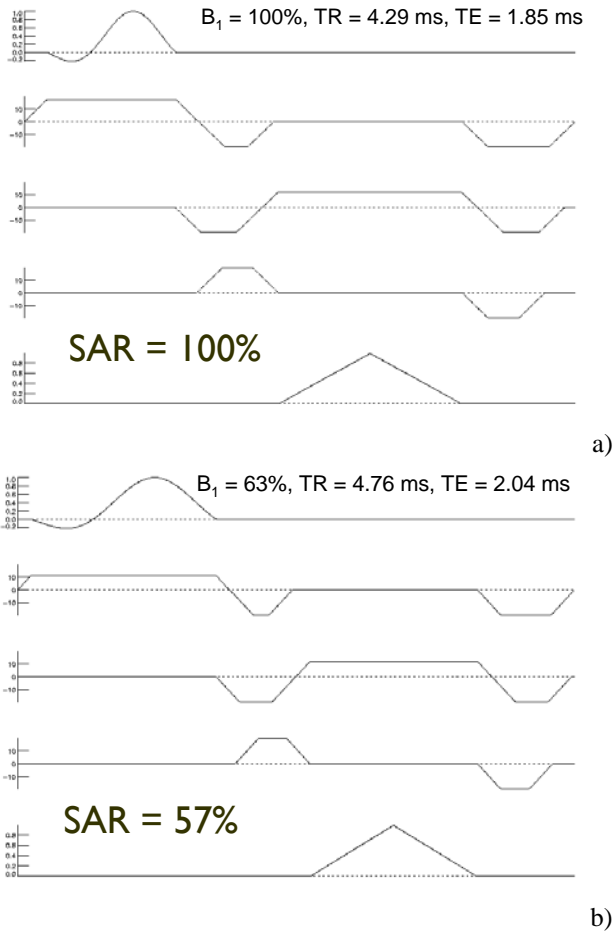


Figure 14 – Same flip angle, lower B_1 , lower SAR, similar scan time.

The Other Sides of Parallel Imaging.

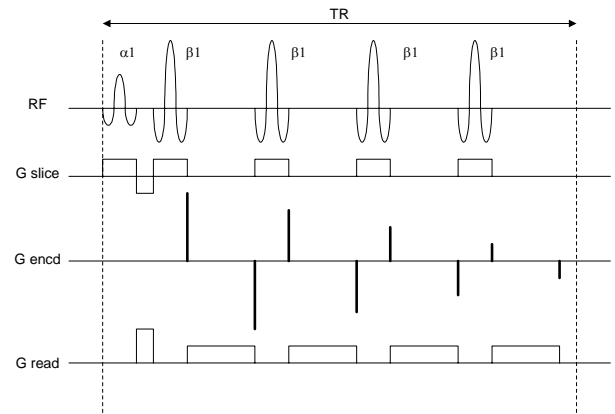
The SENSE parallel imaging method has been available for a number of years. It is primarily associated with scan time reduction. However, it enables many other possibilities.

Figure 15 illustrates an example of how SENSE is used to reduce SAR, Acoustic noise and dB/dt levels. In this discussion we focus mainly on the SAR reduction properties of using SENSE.

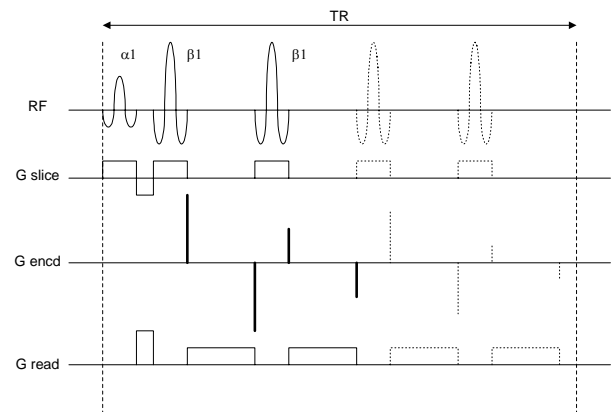
Figure 15a shows a representative gradient and RF timing diagram for a 4 echo Fast Spin Echo (FSE) sequence. In this case, the sequence acquires 4 lines of k-space per TR and uses one 90 degree RF pulse and four 180 degree refocusing RF pulses.

By using SENSE with a reduction factor of, for example, 2, it is possible to drop the last two echoes of the FSE echo

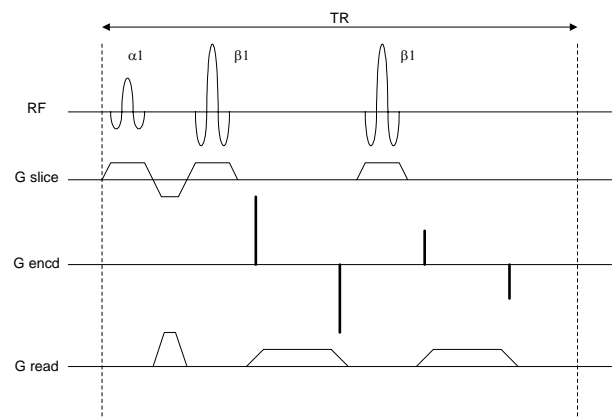
train, see Figure 15b. The SENSE reconstruction, instead, is used to reconstruct the data from the echoes that are not acquired. Clearly, the number of 180 degree RF pulses used in the scan has been reduced by a factor of 2 also. This reduction in the number of RF pulses translates to a significant reduction in the RF duty cycle and, according to the relationship of equation [17], a significant reduction in the deposited SAR.



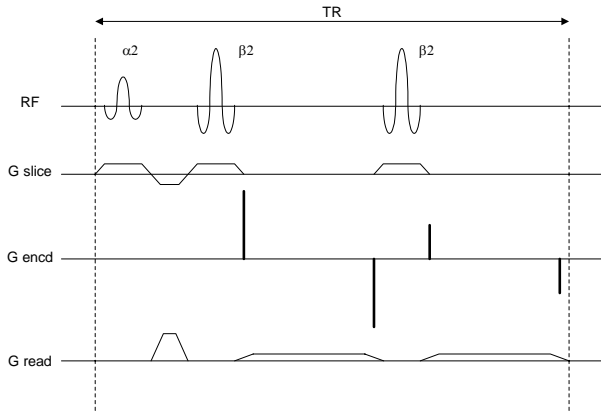
a) Single TR from 4 echo FSE sequence.



b) Same as a) but with SENSE factor 2.



c) Same as b) but with reduced gradient slopes.



d) Same as b) but with lower B_1 .

Figure 15 – The advantages of SENSE for reducing SAR.

This approach can be extended further by utilizing the “dead” time within the TR more effectively. By lengthening gradient slopes, a reduction in acoustic noise levels and dB/dt is achieved, as shown in figure 15c. The additional “dead” time can also be used to lengthen the RF pulses and reduce their amplitude, thereby realizing an additional reduction in SAR with no penalty in scan time. As can be seen, SENSE is an extremely versatile feature that can be used to achieve much more than simply a reduction in scan time.

Flip Angle Sweeps (FAS) in FSE Sequences for SAR Reduction.

As described in the previous section, the Fast Spin Echo (FSE) sequence utilizes a train of refocusing RF pulses following the initial 90 degree RF excitation. It is normal practice that these refocusing RF pulses utilize a flip angle of less than 180 degrees (usually 160 degrees). At 3.0T, even though a lower flip angle is used, the resulting SAR can restrict the maximum number of slices that can be acquired in a single examination. In order to mitigate this issue, the concept of flip angle sweep (FAS) is used (25).

In FSE sequences that use long echo trains, FAS is implemented by starting the refocusing flip angle at a high value (160 degrees) and sweeping this value down, quite quickly, and within the same echo train, to a relatively small flip angle (referred to here as the nominal flip angle). This is illustrated in the diagram of figure 16.

When designing the flip angle sweep, some physical constraints of the NMR spin system must be obeyed. In particular, the flip angle sweep must direct the magnetization to a state of equilibrium that is technically referred to as the “pseudo steady state” (26). Once the “pseudo steady state” has been reached, the resulting lower flip angle can be used throughout the rest of the echo train with very little impact on the image signal to noise (SNR) or quality. However, because a lower flip angle is used for the larger portion of the echo train, the SAR for the scan is

significantly lower. As a result of the SAR reduction from using FAS, many more slices can be acquired and scan efficiency at 3.0T is significantly improved.

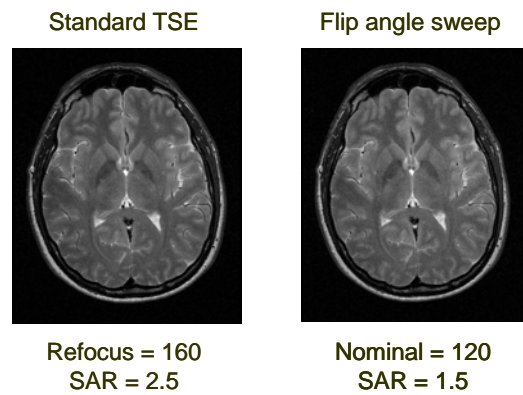
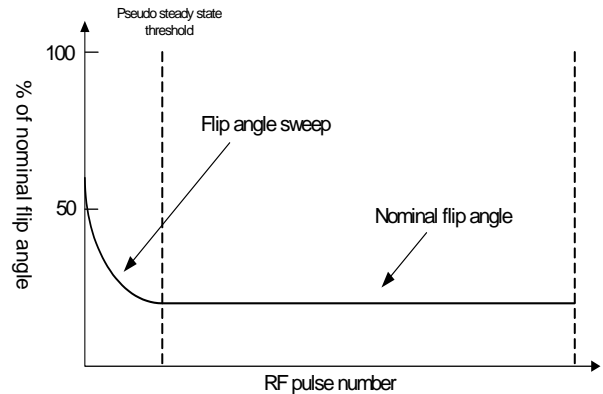


Figure 16 – SAR reduction at 3.0T using Flip Angle Sweep (FAS).

The left side image of figure 16 illustrates a FSE image obtained in the usual manner using 160 degree flip angle refocusing RF pulses throughout. The image on the right side was obtained, using FAS, by sweeping the refocusing flip angle down to 120 degrees. The image quality and contrast remain, while the SAR is reduced significantly.

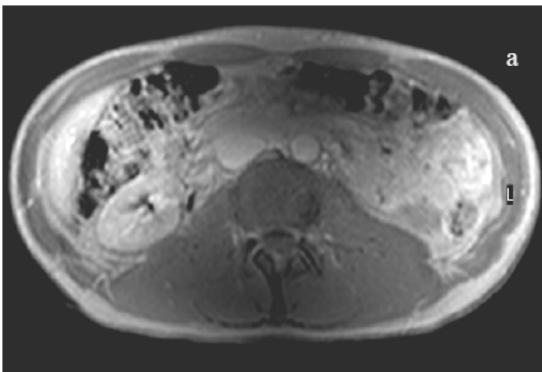
SENSE Based Image Uniformity Correction.

Several data-adaptive methods have been used to try to estimate a non-uniformity field from the image itself. Unfortunately, all of these methods tend to have difficulties in handling images with large ranges of contrast. In the SENSE-based approach this can be solved by using a scan of very low contrast (a proton-density weighted scan). For that scan, the determination of a non-uniformity field is much easier. In practice, a non-uniformity estimate based on such an “easy” scan is applicable to all subsequent scans.

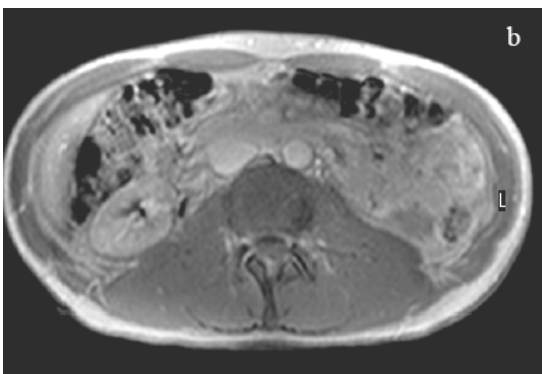
The most robust implementations of SENSE utilize a low-resolution “coarse calibration” reference scan, in order to relate coil-element sensitivity to a reference coil (usually the quadrature RF body coil). This reference scan is designed to be almost purely proton-density weighted.

Using this reference scan, the following procedure can be used for intensity correction:

1. During the planning of the diagnostic scans, a low-resolution density-weighted reference scan is performed, acquiring images from both the phased-array Rx coil array and from the Tx body coil. This results in the image-sets S_i and Q , respectively.
2. By using homomorphic filtering, the image-set Q is uniformity-corrected into an image-set F .
3. The phased-array coil sensitivities are estimated by referring to that uniformity-corrected set F . This results in sensitivity-estimates $s_i = S_i / F$. If only the RF body coil is used for acquisition, its “sensitivity” is estimated as $s_i = Q / F$.
4. The diagnostic scans are reconstructed by the SENSE method, using the knowledge of the aforementioned sensitivities s_i . (In the simple case of one single coil element, this amounts to a division by s_i).



(a) Example intensity shading in body imaging at 3.0T.



(b) Improved uniformity using the advantages of SENSE.

Figure 17 – Using SENSE to improve image uniformity.

Figure 17 shows an example of the improvements in uniformity attainable using the method. This functionality has been available, in clinical practice (one vendor only), for a number of years, and has proven effective in improving image uniformity in body imaging at 3.0T

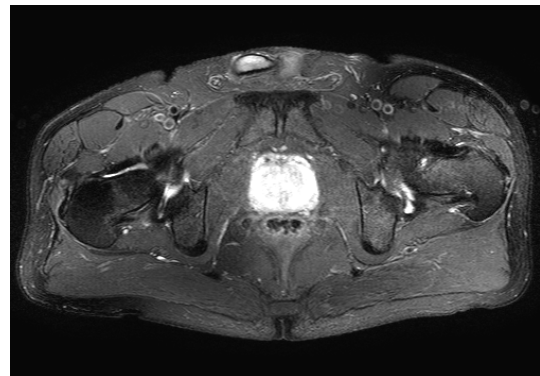
while avoiding the need to “load the patient” with saline bags or off-resonant loops (27).

B₁ Insensitive Fat Suppression (SPAIR).

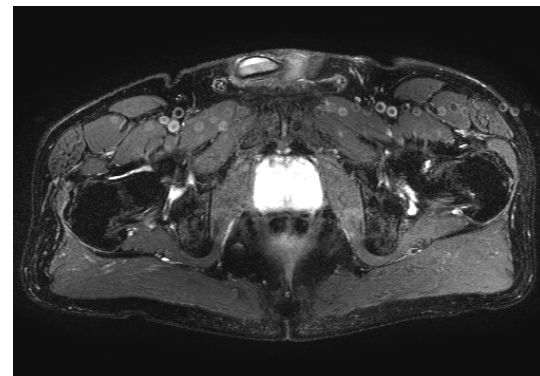
In MRI methods that rely on accurate RF flip angles, the non-uniformities resulting from dielectric effects can become problematic. Spectral fat suppression is one such MRI method.

Spectral fat suppression requires two physical properties to be fulfilled within the object being imaged. It requires a homogeneous B₀ (main magnetic field) and a uniform B₁ (RF transmitting field). If either of these requirements are not fulfilled then a non-uniform fat suppression will result, as shown in figure 18a. To eliminate this problem, new methods of spectral fat suppression have been developed.

One such method developed for 3.0T is called “Spectral selective Attenuated Inversion Recovery”, referred to as SPAIR (28).



(a) Standard spectral fat suppression (3.0T).



(b) Using SPAIR (uniform).

Figure 18 – Improvements in Spectral Fat Suppression at 3.0T using SPAIR.

SPAIR differs from standard spectral fat suppression in that an adiabatic RF pulse is used for the spectral inversion. A particular property of adiabatic RF pulses is that they are relatively immune to B₁ field inhomogeneities and result in a uniform flip angle inside the patient

irrespective of the B_1 uniformity. The improved performance, in this respect, results in a significant improvement of the spectral fat suppression performance at 3.0T, as illustrated in figure 18b.

The Whole is Greater than the Sum of the Parts.

It should be apparent to the reader by now that all the described SAR reduction, image quality, and scan efficiency improvement methods are independent of each other. This independence means that they can be combined. The combination of multiple SAR reduction strategies, in combination with SAR optimized hardware, results in an overall system capability for combined patient safety, scan efficiency and clinical image quality improvement at 3.0T.

Summary.

A brief overview of some of the main technical challenges in high field imaging has been presented. To cover all aspects in more detail would require a complete volume. While comparisons have mostly been made in the context of a 3.0T system, the mechanisms described are equally applicable to higher fields. A number of methods for tackling these challenges have also been presented. While many are routinely available on the high field clinical systems from some manufacturers, it should be clear that parallel imaging, and certain implementations of SENSE, offer major advantages with respect to tackling the challenges that MR imaging at high fields pose. The result of these innovations, together with the technological improvement of MRI hardware, has led to the point where widespread adoption of 3.0T systems is now taking place in clinical practice. Using knowledge, imagination and insight, the possibility exists to design around the physical limitations and to trade one property to solve a different limitation. This bodes well for the improvement of MRI at even higher field strengths.

Acknowledgements.

I would like to acknowledge my colleagues in Best, The Netherlands, Cleveland, U.S.A. and Hamburg, Germany, for their various contributions to this work and their continued effort in meeting the challenges of high field MRI.

References.

[1] Roschmann, P., "RF penetration and absorption in the human body: limitations to high-field whole-body nuclear magnetic resonance imaging", *Med Phys*, 14(6): p. 922-31 (1987).
 [2] Roemer, P.B., et al., "The NMR phased array", *Magn Reson Med.*, 16(2): p. 192-225 (1990).
 [3] Sodickson D.K., Manning W.J., "Simultaneous acquisition of spatial harmonics (SMASH): fast

imaging with radiofrequency coil arrays", *Magn Reson Med.* Oct;38(4):591-603 (1997).
 [4] Pruessmann K.P., Weiger M., Scheidegger M.B., Boesiger P. "SENSE: sensitivity encoding for fast MRI", *Magn Reson Med.* Nov;42(5):952-62 (1999).
 [5] Macovski A., "Noise in MRI", *Magn Reson Med.* 36:494-497 (1996).
 [6] Vlaardingerbroek M.T. & den Boer J.A., "Magnetic Resonance Imaging – Theory and Practise", Springer-Verlag (1999).
 [7] Harvey P.R., Rotem H., Stokar S., "Fat Free Angiography Using Flow Compensated Binomial-Spectral-Spatial-Slice-Variable-Tip-Angle RF Slice Selection", *Proc. Intl. Soc. Mag. Reson. Med.*, Vancouver, p1838 (1997).
 [8] International Standard on the "Particular requirements for the safety of magnetic resonance equipment for medical diagnosis", IEC 60601-2-33, (2002).
 [9] DeMeester G., Zhai Z., Morich M., Harvey P.R., "Head Imaging Using Head Transmit Coil And Body Transmit Coil at 3T", *Proc. Intl. Soc. Mag. Reson. Med.*, Toronto, 2693 (2003).
 [10] Kleihorst R. "A Study of the Effects of SAR on Volunteers", Philips Medical Systems, Internal Report.
 [11] Jin J. and Ji C., "On the SAR and Field Inhomogeneity of Birdcage Coils Loaded with the Human Head", *Mag. Res. Med.* 38:953-963 (1997).
 [12] Collins, C.M., S. Li, and M.B. Smith, "SAR and B_1 field distributions in a heterogeneous human head model within a birdcage coil. Specific energy absorption rate", *Magn Reson Med.*, 40(6): p. 847-56 (1998).
 [13] Harvey P.R., van Hulten H., Zhai, Z., "Quantification of the Spatial Distribution of SAR at 3.0T using MR Thermal Imaging", *Proc. Intl. Soc. Mag. Reson. Med.*, Toronto, 698 (2003).
 [14] Alsop D., et al., "In-vivo B_1 mapping of a Whole-body 3T RF Coil", p1094, ISMRM (2001).
 [15] Zhai Z et al, "Comparison of SAR Properties of 3.0T Body Transmit Coils of Different Lengths", Philips Medical Systems, Internal Report.
 [16] Wilson J.J., Jezzard P., "Utilization of an intracranial diamagnetic passive shim in functional MRI of the inferior frontal cortex", *Magn. Reson. Med.* Nov;50(5):1089-94 (2003).
 [17] Li B.S.U., Regal J., Gonen O., "SNR Versus Resolution in 3D 1H MRS of the Human Brain at High Magnetic Fields", *Magn. Reson. Med.* (2001).
 [18] Thulborn K.R., et al, "Sensitivity Advantage for fMRI at 3.0T over 1.5T", Internet article.
 [19] Farzaneh F., Riederer S.J., Pelc N.J., "Analysis of T2 limitations and off-resonance effects on spatial resolution and artifacts in echo-planar imaging", *Magn Reson Med.* Apr;14(1):123-39 (1990).
 [20] Harvey P.R., Mansfield P., "Avoiding Peripheral Nerve Stimulation: Gradient Wave form Criteria For Optimum Resolution in Echo-Planar Imaging", *Magn Reson Med.*, 32: 236-241 (1994).

- [21] Harvey P.R., Katznelson E., "Modular gradient coil: A new concept in high-performance whole-body gradient coil design", *Magn Reson Med.*, 42(3):561-570 (1999).
- [22] Hebrank, F.X., "SAFE model - A new method for predicting peripheral nerve stimulation in MRI", *Proc. Intl. Soc. Mag. Res. Med.* 8: 2007 (2000).
- [23] Peeren. G., van Eggermond J., Smink J., Engels H., Harvey P.R., "Observed Issues in Predicting Peripheral Nerve Stimulation Caused by Gradient Switching", *Proc. Intl. Soc. Mag. Reson. Med.*, Kyoto, 1664 (2004).
- [24] Edelstein W.A., Hedeem R.A., Mallozzi R.P., El-Hamamsy S.A., Ackermann R.A., and Havens T.J., "Making MRI Quieter", *Magn. Reson. Imaging* 20, p. 155-163 (2002).
- [25] Morakkabati-Spitz N., Gieseke J., Kuhl C., Lutterbey G., von Falkenhausen M., Traber F., Park-Simon TW., Zivanovic O., Schild HH., "MRI of the pelvis at 3 T: very high spatial resolution with sensitivity encoding and flip-angle sweep technique in clinically acceptable scan time", *Eur Radiol.* Oct 14;:1-8 (2005).
- [26] Hennig J., Scheffler K., "Hyperechoes" *Magn Reson Med.*, Jul;46(1):6-12 (2001).
- [27] Schmitt M., Feiweier T., Voellmecke E., Lazar R., Krueger G., Reykowski A., "B₁-Homogenization in abdominal imaging at 3T by means of coupling coils", *Proc. Intl. Soc. Mag. Reson. Med.* 13, p331 (2005).
- [28] De Becker J., Rozijn T., Visser F., Jones A., Beekman W.H., "Silicone Only Breast MRI using a Inversion Recovery TSE sequence with a B₁ independent Spectral Selective Water Suppression Prepulse (SPAIR)", *Proc. Intl. Soc. Mag. Reson. Med.* 13, p1858 (2005).